Microwave Reflectance Studies of Photoelectrochemical Kinetics at Semiconductor Electrodes. 1. Steady-State, Transient, and Periodic Responses

Michael J. Cass,[†] Noel W. Duffy,[‡] Laurence M. Peter,*[,‡] Stephen R. Pennock,[§] Shin Ushiroda,[‡] and Alison B. Walker[†]

Department of Physics, Department of Chemistry, and Department of Electrical Engineering, University of Bath, Bath BA2 7AY, United Kingdom

Received: January 23, 2003; In Final Form: April 21, 2003

Light- and voltage-induced changes in the microwave reflectivity of semiconductors can be used to study the kinetics and mechanisms of electron transfer at semiconductor|electrolyte interfaces. The theory of the method is developed and illustrated by numerical calculations of the steady-state microwave response for low-doped silicon. The results define the range of rate constants that should be experimentally accessible using microwave reflectivity methods. The time and frequency responses of light-induced microwave reflectivity changes are considered, and it is shown that they can be used to derive values of electron transfer and recombination rate constants.

Introduction

The kinetics and mechanisms of electrode processes at metal electrodes have been studied extensively for many years. More recently, outer sphere electron-transfer reactions at semiconductor electrodes in the dark have also been investigated and discussed in the context of current theories of electron-transfer kinetics.[1−7] Conventional electrochemical methods (e.g. potential step, cyclic voltammetry, and ac impedance) rely on potential perturbation of the rates of electrode processes. They can be applied to the study of majority carrier (dark) reactions at semiconductors but are not suitable for characterization of photoelectrochemical processes involving photogenerated minority carriers. Under conditions in which virtually all photogenerated minority carriers are collected, the saturation photocurrent is determined by the light intensity and does not depend on the rate constant for electron transfer, which is expected to be independent of the applied potential.

Since the saturation current at an illuminated semiconductor|electrolyte junction is fixed, the minority carrier concentration at the surface is determined by the rate constant for electron transfer: for the same light intensity, fast electron transfer will lead to a smaller steady-state surface concentration of minority carriers than if electron transfer is slow. In the photocurrent onset region, the potential dependence of the photocurrent is determined by competition between electron transfer and electron−hole recombination (at the surface and in the space charge region). The existence of this competition allows deconvolution of the rate constants for electron transfer and recombination by using frequency (or time) resolved photocurrent methods.[8−10] Examples of experimental methods based on this approach are intensity modulated photocurrent spectroscopy (IMPS)[9−15] and photoelectrochemical impedance spectroscopy (PEIS).[16] In the first method, the intensity of the illumination is modulated sinusoidally, and the magnitude and phase of the photocurrent are measured as a function of modulation frequency. In the second method, which is analogous to conventional impedance spectroscopy, the illumination is constant, and the electrode potential is modulated sinusoidally. However, neither of these methods provides kinetic information about electron transfer in the photocurrent saturation region.

The central problem that any transient or periodic experimental method has to solve is how to distinguish between transport of electrons (or holes) to the interface and interfacial electron transfer. If one considers an experiment in which the illumination of a semiconductor electrode follows a step function, the transient current in the external circuit will reflect the instantaneous displacement current associated with movement of charge carriers. The rise-time of the photocurrent is determined by the *RC* time constant of the system and not by the rate of interfacial electron transfer. What is required is a method that can detect charge carriers "queuing" at the interface to take part in interfacial electron transfer. Detection of these carriers is possible using microwave methods. Microwave reflectance methods are well established for semiconductor characterization,[17−19] but despite the pioneering work of Kunst, Tributsch, and co-workers,[20−28] they have not been widely used in semiconductor electrochemistry. Microwave reflectivity has proved particularly useful for characterizing the silicon|electrolyte interface,[24,26,29−39] although other semiconductors have been studied.[40,41] Our earlier work[30] has shown that frequency resolved light modulated microwave reflectivity measurements can be used to measure the rate constants of electron transfer at illuminated semiconductor|electrolyte interfaces. The present paper extends this approach to the time domain and provides a quantitative theoretical foundation for the analysis of experimental data.

The key point recognized by Tributsch and co-workers[21,42] is the fact that microwave reflectance methods can detect the buildup and decay of minority carriers near the surface of a semiconductor electrode. When a photoelectrode is illuminated under depletion conditions, minority carriers in the space charge region are driven toward the semiconductor|solution interface, where their concentration builds up until a steady-state situation

* Corresponding author. l.m.peter@bath.ac.uk. Fax +44 1225 386502.
[†] Department of Physics.
[‡] Department of Chemistry.
[§] Department of Electrical Engineering.

10.1021/jp030088d CCC: $25.00
Published on Web 05/24/2003

is achieved. Similarly, when the illumination is switched off, the concentration of these excess carriers will fall as they exit across the junction to redox species in the electrolyte. As we show here, the microwave reflectivity response is often dominated by the behavior of the carriers "queuing" at the junction, although the method detects the overall change in conductivity associated with photoexcited minority and majority carriers. This provides an opportunity to study the kinetics of interfacial transfer at illuminated semiconductors. This paper explores these possibilities and presents new insights into the influence of charge-transfer kinetics on the steady-state, transient, and periodic microwave responses. The methods described here have been applied to study the hydrogen evolution reaction (HER) on p-Si in acidic fluoride media[43] as well as the photoreduction of $Ru(NH_3)_6^{3+}$ at p-Si, which appears to proceed via the hydrogen intermediate formed in the HER.[44]

Theoretical Basis

Light-Induced Changes in Microwave Reflectivity. The microwave power reflected from the rear of a semiconductor sample depends on the complex dielectric properties (dielectric constant and conductivity) of the sample and solution. Perturbation of the semiconductor|electrolyte system by light alters the local dielectric properties primarily as the result of changes in the local concentration of free carriers (electrons and holes). The change in the reflected microwave power ΔR_M can be related to the change in the conductivity of the sample.[42] ΔR_M is defined as

$$\Delta R_M = \frac{\Delta P_r}{P_{in}} \tag{1a}$$

Here ΔP_r is the change in reflected microwave power, and P_{in} is the incident microwave power. Since the reflected power P_r depends on the microwave reflectivity R_M, eq 1a can be rewritten as

$$\Delta R_M = R_M \frac{\Delta P_r}{P_r} \tag{1b}$$

For laterally homogeneous semiconductors under homogeneous illumination, ΔR_M is determined by the change in local conductivity caused by illumination. The mean value of this conductivity change, $\langle \Delta\sigma \rangle$, can be calculated by integrating the profiles of excess electrons and holes in the sample: ($\Delta n(x)$ and $\Delta p(x)$). It has been proposed that the measured microwave response is a linear function of the mean conductivity change,[42] so that

$$\Delta R_M = S\langle \Delta\sigma \rangle = \frac{S}{d}\int_0^d \Delta\sigma(x)\,dx = \frac{Sq}{d}\int_0^d [\mu_n \Delta n(x) + \mu_p \Delta p(x)]\,dx \tag{2}$$

Here S is the sensitivity factor with units Ω cm, $\langle \Delta\sigma \rangle$ is the mean conductivity change, $\Delta\sigma(x)$ is the position dependent change in conductivity, d is the sample thickness, and μ_n and μ_p are the electron and hole mobilities. It should be noted here that the mobilities could be lower than the values characteristic of the bulk semiconductor if accumulation or inversion layers are formed.[45−48] In principle, S can be calculated using the Fresnel equations[17] (see below), but it is usually more convenient to measure it experimentally. Its magnitude and sign depend on the thickness and doping of the sample as well as on the microwave frequency.

To obtain the microwave reflectivity response, it is necessary to calculate the excess profiles $\Delta n(x)$ and $\Delta p(x)$ by solving the continuity equations and Poisson's equation with appropriate boundary conditions. Schlichthörl and Lewerenz have used an analytical approach to compute minority carrier profiles.[25] The more general numerical approach that is used here includes the effects of interfacial electron transfer, recombination in the space charge region, and recombination at the rear contact. In principle, it is not necessary to make the assumption of a linear relationship between ΔR_M and the mean conductivity change (cf. eq 2). If the electron and hole profiles are known, a multilayer model based on solution of the Fresnel equations can be used to calculate the reflectance. We have also explored this approach in order to establish the validity of the linear approximation under different conditions.

Calculation of the Steady-State Excess Carrier Distributions. To calculate the carrier profiles, it is necessary to solve the continuity equations, the current density equations, and Poisson's equation self-consistently. The continuity equations in one dimension and under steady-state conditions are

$$\frac{1}{q}\frac{dj_p}{dx} = \frac{-1}{q}\frac{dj_n}{dx} = \alpha I_0 e^{-\alpha x} - \frac{np - n_i^2}{\tau_p(n + n_i) + \tau_n(p + n_i)} \tag{3}$$

Here q is the electronic charge, j_n and j_p are the electron and hole current densities, α is the absorption coefficient, I_0 is the incident photon flux density, n and p are the local densities of electrons and holes, τ_n and τ_p are the electron and hole lifetimes, and n_i is the intrinsic carrier density. The first term on the right-hand side of the above equation represents the rate of photogeneration of carriers, and the second term the rate of volume recombination in the Hall, Shockley, and Read formalism.[49,50] Here we make the common simplifying assumption that the recombination centers are located in the midgap where the recombination rate is maximum.

The carrier densities can be expressed in the form

$$n = N_C \exp\left(\frac{E_{Fn} - E_C}{k_B T}\right) \tag{4a}$$

$$p = N_V \exp\left(\frac{-E_{Fp} + E_C - E_g}{k_B T}\right) \tag{4b}$$

where N_C and N_V are the effective density of states in the conduction and valence bands, respectively, E_{Fn} and E_{Fp} are the electron and hole quasi-Fermi energies, E_C is the conduction band edge, and E_g is the energy band gap (see the Appendix).

Using the Einstein relation, the current−density equations can be expressed as

$$j_n = -\mu_n n \frac{dE_{Fn}}{dx} \tag{5a}$$

$$j_p = -\mu_p p \frac{dE_{Fp}}{dx} \tag{5b}$$

where μ_n and μ_p are the electron and hole mobilities.

Poisson's equation can be written in the form

$$\frac{dD}{dx} = q(p - n + N_D - N_A) \tag{6}$$

where D is the electric displacement, N_D is the donor density, and N_A is the acceptor density.

A self-consistent solution to these equations can be obtained numerically. The boundary conditions are defined by the fact that the semiconductor has an electrolyte Schottky contact on one side and a metallic ohmic contact on the other. For the Schottky electrolyte contact, the boundary conditions are

$$j_n(0) = qk_{tr}(n - n_{eq}) \tag{7a}$$

$$j_p(0) = -qk_{tr}(p - p_{eq}) \tag{7b}$$

$$E_C(0) = \Phi_{Bn} \tag{7c}$$

where Φ_{Bn} is the Schottky barrier height, n_{eq} and p_{eq} are the equilibrium carrier densities at the surface, and k_{tr} is the emission/recombination velocity across the barrier, which is equivalent to a pseudo-first-order heterogeneous electron-transfer rate constant (cm s^{-1}). In fact, of course, electron transfer from conduction band states in a semiconductor to redox species in the solution is a second-order heterogeneous process because the rate depends on the concentration of redox species (cm^{-3}) and the concentration of minority carriers in the surface region (cm^{-3}). The rate constant therefore has units of cm^4 s^{-1}. However, for constant concentrations of redox species in the absence of diffusion limitations, the process becomes pseudo-first-order heterogeneous, and the rate constant is equivalent to v_r, with units of cm s^{-1}. Using the analogy of surface state recombination, k_{tr} can also be expressed in terms of the thermal velocity of minority carriers, v_{th}, and the surface density (N_{redox}) and cross section (σ_{redox}) of the redox species.[7]

$$k_{tr} = v_{th}\sigma_{redox}N_{redox} \tag{8a}$$

If the concentration of excess minority carriers in the tunneling region of thickness δ close to the surface is expressed as a concentration per unit area, $\Delta n_{surf} = \Delta n(0)\delta$, a rate constant for interfacial electron transfer with units s^{-1} can be defined as

$$k_1 = \frac{k_{tr}}{\delta} = \frac{v_{th}\sigma_{redox}N_{redox}}{\delta} \tag{8b}$$

This simple first-order rate constant appears in many treatments of photoelectrochemical kinetics and is used, for example, in the phenomenological analysis of IMPS responses.[14]

The boundary conditions for the ohmic back-contact are

$$E_C(d) = q(U_{fb} - U) \tag{9a}$$

$$E_{Fn}(d) = E_{Fp}(d) = q(U - U_{redox}) \tag{9b}$$

where U is the electrode potential, U_{redox} is the redox potential, and U_{fb} is the flatband potential (it is assumed that the potential drop in the Helmholtz layer is independent of applied potential).

The carrier profiles were calculated numerically for the p-Si|electrolyte junction using an iterative relaxation method.[51] Details of the parameter values used in the calculation are given in the Appendix.

Results and Discussion

Electron and Hole Profiles. Figure 1 illustrates the influence of the electron-transfer rate constant on the profiles of excess electrons and holes. The calculations were performed for a band bending $q(U - U_{fb}) = -0.5$ eV, which corresponds to the photocurrent saturation region where recombination is negligible. The double logarithmic representation allows visualization of the electron and hole concentrations close to the surface as well as in the space charge region and quasi-neutral region. The Beer Lambert photogeneration profile corresponding to the first term on the right-hand side of eq 3 is also shown in the figure to indicate the penetration depth of the light ($\lambda = 626$ nm). Figure 1 suggests that the concentration of electrons located close to the surface depends linearly on the rate constant for electron transfer, as expected in the photocurrent saturation region. Only a small part of the accumulated electron charge is balanced by accumulation of holes outside the space charge region; a much larger residual component of the balancing charge will appear in the contacting electrolyte phase, forming a double layer. In practice, this accumulation of charge can lead to a substantial change in the potential distribution across the system. As we show elsewhere,[52] the resulting band edge unpinning can be detected by transient photocapacitance measurements.

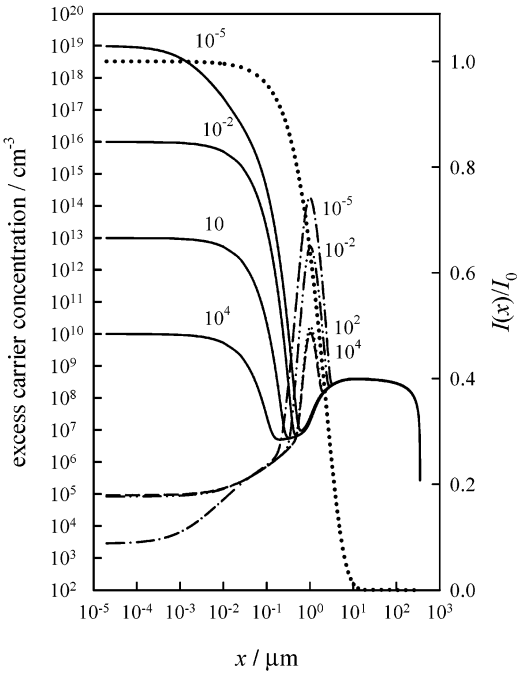

Figure 1. Excess carrier profiles and photogeneration rate calculated for the low-doped p-Si|electrolyte junction for a band bending of 0.5 eV and an incident photon flux of 10^{14} cm^{-2} s^{-1} at 626 nm. Note the double logarithmic scale. Solid lines: excess electron density. Broken lines: excess hole density. The local photon flux $I(x) = I_0 \exp(-\alpha x)$ is also shown (broken line: right-hand scale). See the Appendix for parameter values. The figure illustrates the effect of changing the rate constant for interfacial electron transfer (values of k_{tr} shown in cm s^{-1}).

The potential dependence of the electron and hole profiles is illustrated in Figure 2. At low values of band bending, the excess carrier densities are small, as a consequence of recombination in the space charge region. As the band bending is increased, recombination becomes less important, and the excess carrier concentration densities increase.

Current Voltage Characteristics. In the absence of surface recombination, the photocurrent density will be determined by the product of the concentration of excess minority carriers at the surface and the rate constant for interfacial electron transfer. Figure 3 compares the shape of the photocurrent voltage plots, calculated for different values of the electron-transfer rate constant, with the limiting behavior predicted by the Gärtner equation[53] (no recombination).

$$\frac{j_{photo}}{qI_0} = 1 - \frac{\exp(-\alpha W)}{1 + \alpha L_n} \tag{10a}$$

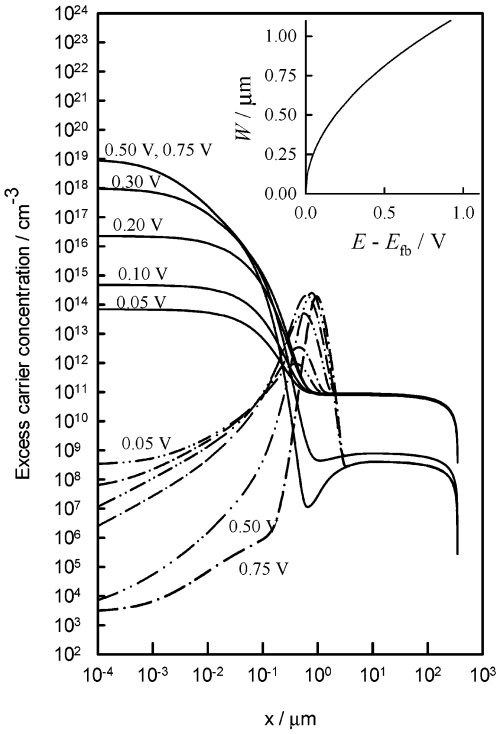

Figure 2. Excess electron and hole profiles calculated as a function of band bending. Solid lines: excess electron density. Broken lines: excess hole density. Band bending in eV as shown. The inset shows the potential dependence of the width of the space charge region. $k_{tr} = 10^{-5}$ cm s^{-1}. Incident photon flux (626 nm) = 10^{14} cm^{-2} s^{-1}.

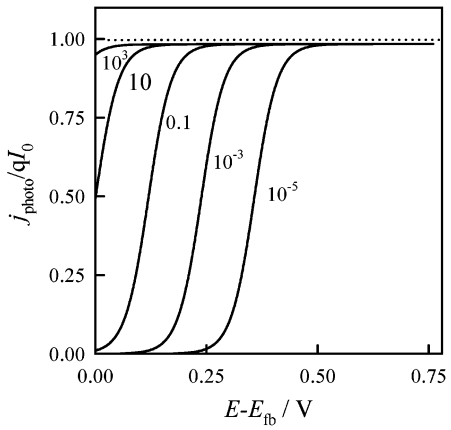

Figure 3. Normalized photocurrent voltage curves calculated for different values of the electron-transfer rate constant, k_{tr} (values shown in cm s^{-1}). Incident photon flux = 10^{14} cm^{-2} s^{-1}. See the Appendix for other parameter values. The delayed onset is due to recombination of electrons and holes in the space charge region. The broken line shows the normalized photocurrent calculated from the Gärtner equation. Note that space charge recombination becomes negligible when k_{tr} is larger than 10^3 cm s^{-1}.

Here L_n is the electron diffusion length and W is the width of the space charge region given by

$$W = \left(\frac{2\epsilon\epsilon_0\Delta\phi_{sc}}{qN_A}\right)^{1/2} \qquad (10b)$$

It can be seen that the $j-V$ characteristic predicted by the Gärtner equation corresponds to an incident photon to current conversion efficiency (IPCE) of almost unity over the entire potential range because the electron diffusion length in low-doped silicon is comparable with the sample thickness (350 μm).

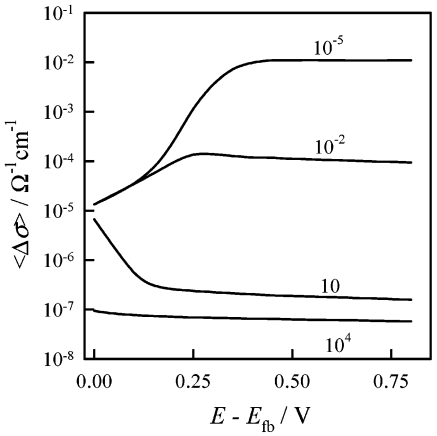

Figure 4. Potential dependence of the light-induced change in mean conductivity $\langle\Delta\sigma\rangle$ of a silicon sample under illumination (10^{14} cm^{-2} s^{-1}) for different values of the electron-transfer rate constant, k_{tr} (values shown in cm s^{-1}). The light-induced change in conductivity determines the microwave response (cf. eq 1). Note that an increase in conductivity (and hence microwave response) only occurs in the depletion region if k_{tr} is less than 1 cm s^{-1}.

By contrast, the plots calculated using the HSR model are characterized by a delayed onset of the photocurrent that indicates that electrons are being lost by recombination rather than transferring across the interface. As k_{tr} becomes smaller, the photocurrent onset is displaced away from the flatband potential.

Conductivity Changes. The change in mean conductivity brought about by illumination depends on the integral of the excess electron and hole densities (cf. eq 2). The potential dependence of the mean conductivity change for different values of the rate constant for electron transfer is shown in Figure 4. If the relationship between ΔR_M and $\langle\Delta\sigma\rangle$ is linear, as implied by eq 2, the corresponding changes in microwave reflectivity can be calculated from the figure if the sensitivity factor, S, has been determined experimentally or has been calculated (see below).

The magnitude of the light-induced change in conductivity (and hence the microwave response) under depletion conditions is expected to depend on the rate constant for electron transfer. Figure 5 illustrates the dependence of $\langle\Delta\sigma\rangle$ for a wide range of values of the charge-transfer rate constant, k_{tr}. It is evident from the plot that, for the case of very rapid charge transfer, the change in conductivity tends toward a limiting value. This is associated with photogenerated carriers located outside the space charge region, since if charge transfer is rapid, minority carriers inside the space charge region are swept to the surface, where they are extracted rapidly, preventing any significant build up. This limit corresponds to the Gärtner equation. In practice, of course, the range of rate constants that can be determined from the light-induced microwave response will be smaller than the range plotted here, since the sensitivity limit corresponds to reflectivity changes of around 1 part per million.

The change in microwave reflectivity can be calculated without making the a priori assumption of a linear relationship between ΔR_M and $\langle\Delta\sigma\rangle$. This was done using a filter stack model to map the carrier concentration, and hence the local conductivity, in a series of thin layers of constant dielectric constant and variable conductivity. The electron and hole distributions in the dark and under illumination were used to calculate the mean conductivity in a series of layers with progressively increasing thickness (see the Appendix). The microwave response was obtained from the difference between the reflectance values calculated for illuminated and dark conditions. The results of

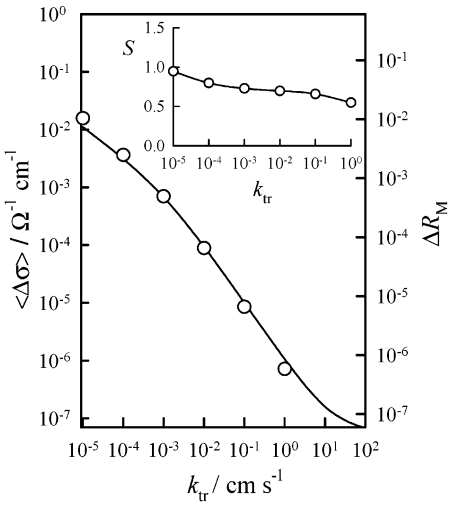

Figure 5. Solid line: dependence of the change in mean conductivity $\langle\Delta\sigma\rangle$ on the rate constant for interfacial charge transfer, calculated from the excess carrier profiles. Open circles: values of the microwave reflectance change calculated using a multilayer model and the Fresnel equations. Note the close correspondence between the results obtained by the two methods over a wide range of rate constant values, indicating that the linear approximation implicit in eq 2 is quite satisfactory. The inset shows that the sensitivity factor varies by less than a factor of 2 over 6 orders of magnitude of k_{tr}.

calculations performed for a range of electron transfer rate constants have also been included in Figure 5 for comparison. It can be seen that the linear approximation (eq 2) is reasonably satisfactory over the range in which the modulated microwave response is measurable. The sensitivity factor, S, can be derived by comparing the calculated changes in $\langle\Delta\sigma\rangle$ as a function of k_{tr} with the corresponding values of ΔR_M from the Fresnel calculation. The inset to Figure 5 shows the result. The variation of S is remarkably small. For order of magnitude calculations at least, its value can be taken as 1.0 Ω cm for low-doped p-type Si samples ($N_A = 10^{15}$ cm^{-3}). If we take a practical lower resolution limit of 10^{-6} for ΔR_M, it follows from Figure 5 that rate constants up to about 1 cm s^{-1} are accessible to measurement.

As noted previously, the electron or hole mobility is reduced under accumulation or inversion conditions, and we may therefore expect deviations from the theoretical plots shown in Figure 5 in the case of very slow electron transfer, where minority carrier concentrations at the surface become high (cf. Figure 1).

Transient and Periodic Microwave Responses. We consider the photocurrent and microwave responses to an illumination step under conditions in which recombination and series resistance effects are negligible (i.e. in the photocurrent saturation region). The movement of photogenerated carriers gives rise to an instantaneous displacement current, and consequently, the photocurrent measured in the external circuit follows the light step. It is not possible to distinguish between electrons that are present in the space charge region of the semiconductor and those that have been transferred to species in the electrolyte, so the photocurrent response contains no kinetic information. By contrast, the microwave response does contain kinetic information because, as the foregoing treatment shows, it detects the electrons "queuing" at the interface in the semiconductor. When the light is switched on, photogenerated electrons are displaced toward the surface, where they can take part in an electron transfer reaction to redox species in solution. The electron density at the surface will build up to a steady state

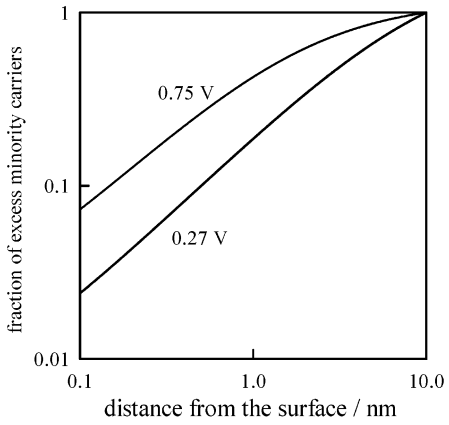

Figure 6. Fraction of the total number of excess minority carriers located within a distance x of the surface plotted as a function of x. Values of band bending as shown; light intensity = 10^{14} cm^{-2} s^{-1}; k_{tr} = 10^{-5} cm s^{-1}. Note that nearly all of the excess minority carriers are located within 10 nm of the surface.

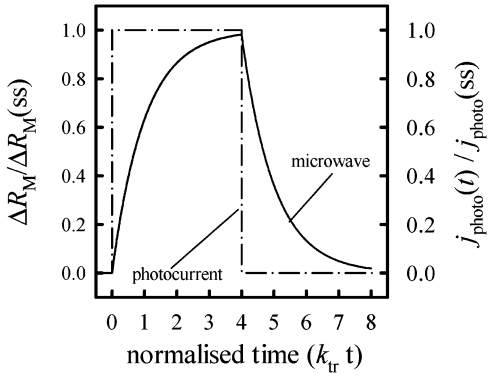

Figure 7. Normalized time dependence of the surface excess minority carrier density showing the buildup and decay as the light is switched on and off, respectively. The time constant is the inverse of the first-order rate constant k_1 (s^{-1}) for the interfacial electron transfer process. Note that the photocurrent response is essentially instantaneous (*RC* effects are neglected).

with a time constant determined by the rate constant for interfacial charge transfer. A full time-dependent solution of this problem is possible, but it is convenient to take a simpler approach. The carrier profiles shown in Figure 1 indicate that the excess electron concentration increases steeply near the surface, so that the conductivity change arises predominantly from this region. This conclusion is reinforced by Figure 6, which shows the cumulative total of minority carriers, as a function of distance for a case where electron transfer is slow, so that a large buildup of electrons occurs. It can be seen that nearly all of the excess electrons are located within 10 nm of the interface, so that they will behave essentially as a surface charge. It follows that the transient microwave response under non-steady-state conditions will reflect the buildup and decay of these "near-surface" electrons. In this case, the time constant for the buildup and decay is given by the inverse of the first-order rate constant defined in eq 8b.

In the photocurrent saturation region, where recombination is negligible, the microwave response to a square pulse of illumination should therefore follow the simple shape shown in Figure 7. If carriers are also consumed by recombination in the space charge region or at the surface, the decay rate constant will become ($k_1 + k_{rec}$), where k_{rec} is a phenomenological rate constant that accounts for both surface and space charge recombination.

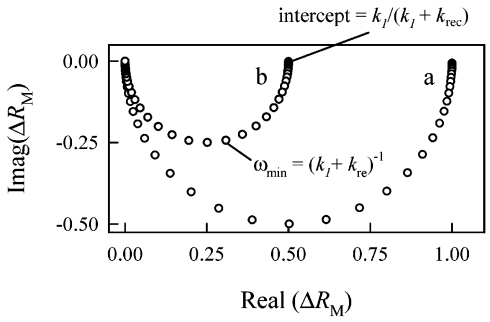

Figure 8. Schematic normalized light modulated microwave reflectivity (LMMR) responses plotted in the complex plane (a) for a potential in the photocurrent saturation region and (b) for a potential corresponding to a photocurrent of half the saturation value. The minimum of the response occurs at an angular frequency equal to the sum of the rate constants for electron transfer and recombination (cf. eq 11).

The microwave response to intensity-modulated light should also show first-order behavior with a time constant determined by the sum $(k_1 + k_{rec})$.[10,30] In practice, it is convenient to normalize the plots with respect to the limiting low-frequency microwave response in the absence of recombination, that is, in the photocurrent saturation region. The normalized microwave response to sinusoidal modulation of the light intensity is given by

$$\mathrm{Re}(\Delta R_M) = \frac{k_{tr}(k_{tr} + k_{rec})}{(k_{tr} + k_{rec})^2 + \omega^2} \tag{11a}$$

$$\mathrm{Im}(\Delta R_M) = \frac{k_{tr}\omega}{(k_{tr} + k_{rec})^2 + \omega^2} \tag{11b}$$

Figure 8 compares the normalized complex plane LMMR plots in the saturation and onset regions of the photocurrent voltage curve where half of the minority carriers are lost by recombination. The most important point to note here is that a semicircular LMMR response is observed in the photocurrent saturation region where the periodic photocurrent response is in phase with the excitation. This contrasts with the intensity modulated photocurrent (IMPS) response, which contracts to a point on the real axis because the photocurrent is in phase with the illumination. As shown elsewhere,[30] the minimum frequency ω_{min} in the LMMR response is equal to the sum of k_1 and k_{rec}, and the normalized low-frequency intercept on the real axis of the LMMR plot is given by the ratio $k_1/(k_1 + k_{rec})$. The value of k_1 determined in this way can be compared with the value of k_{tr} derived by comparing the magnitude of the limiting low-frequency microwave response with the predictions of the modeling approach outlined in the first part of this paper. Such a comparison can be used to check the validity of the first-order approximation based on the use of surface concentrations of minority carriers (cf. eq 8b). These comparisons have been used in a study of hydrogen evolution at p-Si that is reported elsewhere.[43]

Conclusions

This exploration of the theoretical aspects of the microwave reflectivity method indicates that steady-state as well as time and frequency resolved microwave methods can provide information about charge-transfer kinetics at semiconductor|electrolyte interfaces. Calculation of the magnitude of the dc limit of the microwave response from first principles has established a direct correlation with the rate of electron transfer. This opens the way to comparison of steady-state and modulated microwave reflectance data. The analysis given here should provide a sound theoretical basis for more widespread application of microwave reflectance methods in semiconductor photoelectrochemistry.

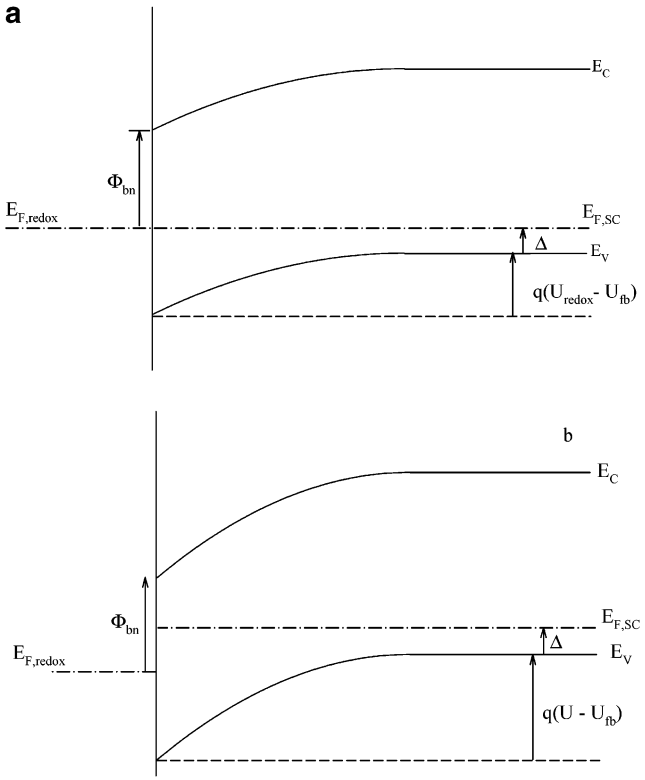

Figure 9. Illustration of the band bending and relevant energies for the p-Si|electrolyte junction; (a) the equilibrium situation; (b) the situation for an applied electrode potential that is more negative than the potential of the redox system.

Acknowledgment. This work was supported by the U.K. Science and Engineering Research Council.

Appendix

Figure 9 illustrates the equilibrium band bending and the band bending for an electrode potential (U) more negative than the equilibrium potential. U_{fb} is the flat band potential. The following parameter values were used in the numerical calculations of excess electron and hole distributions. T, absolute temperature: 300 K. ϵ_s, dielectric constant of Si: 11.9. N_c, conduction band density of states: 2.8×10^{19} cm^{-3}. N_v, valence band density of states: 1.0×10^{19} cm^{-3}. E_g, band gap: 1.12 eV. N_D, donor density: 0.0 cm^{-3}. N_A, acceptor density: 1.0×10^{15} cm^{-3}. Φ_{Bn}, Schottky barrier height: 0.5 eV (approximate value for the hydrogen redox system). τ_n, electron lifetime: 1.0×10^{-4} s. τ_p, hole lifetime: 1.0×10^{-4} s. μ_n, electron mobility: 1350 cm^2 V^{-1} s^{-1}. μ_p, hole mobility: 480 cm^2 V^{-1} s^{-1}. m^*_n, effective electron mass: $1.02m_0$. m^*_p, effective hole mass: $0.52m_0$. α_{626}, absorption coefficient at 626 nm: 4.42×10^3 cm^{-1}.

The calculations of the microwave reflectivity were carried out using a model with 11 layers. Nine layers were used to model the distance dependent conductivity of the sample, and the remaining two layers represented the air and electrolyte phases. Starting from the Si|electrolyte interface, the thicknesses of the first seven layers in the silicon were (nm) 1, 9, 40, 50, 150, 250, and 500. The final two layers were 9 and 340 μm thick, followed by the air filled waveguide. The conductivity

in the layers was obtained from the profiles of total electron and hole density calculated for dark and illuminated conditions.

References and Notes

(1) Meier, A.; Kocha, S. S.; Hanna, M. C.; Nozik, A. J.; Siemoneit, K.; ReinekeKoch, R.; Memming, R. *J. Phys. Chem. B* **1997**, *101*, 7038.

(2) Meier, A.; Selmarten, D. C.; Siemoneit, K.; Smith, B. B.; Nozik, A. J. *J. Phys. Chem. B* **1999**, *103*, 2122.

(3) Meier, A.; Selmarten, D.; Hanna, M.; Nozik, A.; Siemoneit, K.; Reineke-Koch, R.; Memming, R. *Z. Phys. Chem.* **1999**, *213*, 117.

(4) Lewis, N. S. *J. Phys. Chem. B* **1998**, *102*, 4843.

(5) Royea, W. J.; Fajardo, A. M.; Lewis, N. S. *J. Phys. Chem. B* **1998**, *102*, 3653.

(6) Pomykal, K. E.; Fajardo, A. M.; Lewis, N. S. *J. Phys. Chem.* **1996**, *100*, 3652.

(7) Morrison, S. R. *Electrochemistry of semiconductor and metal electrodes*; Plenum Press: New York, 1980.

(8) Peter, L. M. *Chem. Rev.* **1990**, *90*, 753.

(9) Peter, L. M. Photoelectrochemical kinetics at semiconductor electrodes. In *Comprehensive chemical kinetics*; Hancock, G., Ed.; Elsevier: Amsterdam, 1999; Vol. 37; p 223.

(10) Peter, L. M.; Vanmaekelbergh, D. Time and Frequency Resolved Techniques in Photoelectrochemistry. In *Advances in Electrochemical Science and Engineering*; Alkire and Kolb, D. M., Ed.; VCH Wiley: Weinheim, 1999; Vol. 6, p 77.

(11) Peter, L. M.; Li, J.; Peat, R. *J. Electroanal. Chem.* **1984**, *165*, 29.

(12) Li, J.; Peat, R.; Peter, L. M. *J. Electroanal. Chem.* **1984**, *165*, 41.

(13) Ponomarev, E. A.; Peter, L. M. *J. Electroanal. Chem.* **1995**, *396*, 219.

(14) Peter, L. M.; Ponomarev, E. A.; Fermin, D. J. *J. Electroanal. Chem.* **1997**, *427*, 79.

(15) Fermin, D. J.; Ponomarev, E. A.; Peter, L. M. *J. Electroanal. Chem.* **1999**, *473*, 192.

(16) Ponomarev, E. A.; Peter, L. M. *J. Electroanal. Chem.* **1995**, *397*, 45.

(17) Kunst, M.; Beck, G. *J. Appl. Phys.* **1986**, *60*, 3558.

(18) Kunst, M.; Sanders, A. *Semiconductor Sci. Technol.* **1992**, *7*, 51.

(19) Wunsch, F.; Schlichthörl, G.; Tributsch, H. *J. Phys. D* **1993**, *26*, 2041.

(20) Kunst, M.; Beck, G.; Tributsch, H. *J. Electrochem. Soc.* **1984**, *131*, 954.

(21) Tributsch, H.; Schlichthörl, G.; Elstner, L. *Electrochim. Acta* **1993**, *38*, 141.

(22) Schlichthörl, G.; Tributsch, H. *Electrochim. Acta* **1992**, *37*, 919.

(23) Lewerenz, H. J.; Schlichthörl, G. *J. Electroanal. Chem.* **1992**, *327*, 85.

(24) Lewerenz, H. J.; Schlichthörl, G. *J. Appl. Phys.* **1994**, *75*, 3544.

(25) Schlichthörl, G.; Lewerenz, H. J. *J. Electroanal. Chem.* **1998**, *443*, 9.

(26) Wunsch, F.; Nakato, Y.; Kunst, M.; Tributsch, H. *J. Chem. Soc., Faraday Trans.* **1996**, *92*, 4053.

(27) Chaparro, A. M.; ColbeauJustin, C.; Kunst, M.; Tributsch, H. *Semiconductor Sci. Technol.* **1998**, *13*, 1472.

(28) Chaparro, A. M.; Tributsch, H. *J. Phys. Chem. B* **1997**, *101*, 7428.

(29) Schlichthörl, G.; Peter, L. M. *J. Electrochem. Soc.* **1994**, *141*, L171.

(30) Schlichthörl, G.; Ponomarev, E. A.; Peter, L. M. *J. Electrochem. Soc.* **1995**, *142*, 3062.

(31) Schlichthörl, G.; Peter, L. M. *J. Electrochem. Soc.* **1995**, *142*, 2665.

(32) Schlichthörl, G.; Peter, L. M. *J. Electroanal. Chem.* **1995**, *381*, 55.

(33) Cattarin, S.; Chazalviel, J. N.; Da Fonseca, C.; Ozanam, F.; Peter, L. M.; Schlichthörl, G.; Stumper, J. *Proc. Electrochem. Soc.* **1997**, *97*−*20*, 228.

(34) Cattarin, S.; Chazalviel, J. N.; Da Fonseca, C.; Ozanam, F.; Peter, L. M.; Schlichthörl, G.; Stumper, J. *J. Electrochem. Soc.* **1998**, *145*, 498.

(35) Böhm, S.; Peter, L. M.; Schlichthörl, G.; Greef, R. *J. Electroanal. Chem.* **2001**, *500*, 178.

(36) Natarajan, A.; Oskam, G.; Oursler, D. A.; Searson, P. C. *Mater. Res. Soc. Symp. Proc.* **1997**, *451*, 197.

(37) Natarajan, A.; Oskam, G.; Searson, P. C. *J. Appl. Phys.* **1998**, *83*, 2112.

(38) Natarajan, A.; Nellore, A.; Searson, P. C. *J. Appl. Phys.* **1999**, *85*, 1631.

(39) Rauscher, S.; Nast, O.; Jungblut, H.; Lewerenz, H. J. *Proc. Electrochem. Soc.* **1998**, *97*−*35*, 439.

(40) Chaparro, A. M.; Ellmer, K.; Tributsch, H. *Electrochim. Acta* **1999**, *44*, 1655.

(41) Thomas, B.; Ellmer, K.; Bohne, W.; Rohrich, J.; Kunst, M.; Tributsch, H. *Solid State Commun.* **1999**, *111*, 235.

(42) Tributsch, H. Microwave (Photo)electrochemistry. In *Modern Aspects of Electrochemistry*; White, R. E., Ed.; Kluwer Academic/Plenum Publishers: New York, 1999; Vol. 33, p 435.

(43) Cass, M. J.; Duffy, N. W.; Peter, L. M.; Pennock, S. R.; Ushiroda, S.; Walker, A. B. Submitted to *J. Phys. Chem. B*, **2003**, *107*, 5864.

(44) Cass, M. J.; Duffy, N. W.; Peter, L. M.; Pennock, S. R.; Ushiroda, S.; Walker, A. B. In preparation.

(45) Elmiger, J. R.; Kunst, M. *Appl. Phys. Lett.* **1996**, *69*, 517.

(46) Kunst, M.; Abdallah, O.; Wunsch, F. *Sol. Energy Mater. Sol. Cells* **2002**, *72*, 335.

(47) Schlichthörl, G.; Peter, L. M. *J. Electrochem. Soc.* **1995**, *142*, 2665.

(48) Mudanai, S.; Chindalore, G. L.; Shih, W. K.; Wang, H.; Ouyang, Q.; Tasch, A. F.; Maziar, C. M.; Banerjee, S. K. *IEEE Trans. Electron Devices* **1999**, *46*, 1749.

(49) Landsberg, P. Cambridge University Press: Cambridge, 1991; p 102.

(50) Sze, S. M. *Physics of Semiconductor Devices*, 2nd ed.; John Wiley & Sons: New York, 1981.

(51) Press, W. H.; Flannery, B. P.; Teukolsky, S. A. *Numerical Recipes in C*; Cambridge University Press: Cambridge, 1988.

(52) Peter, L. M.; Ushiroda, S. In preparation.

(53) Gärtner, W. W. *Phys. Rev.* **1959**, *116*, 84.